# Optical and electrical study of organic solar cells with a 2D grating anode

**Wei E.I. Sha,**[1] **Wallace C.H. Choy,**[1,*] **Yumao Wu,**[1] **and Weng Cho Chew**[1,2]

[1]*Department of Electrical and Electronic Engineering, The University of Hong Kong, Pokfulam Road, Hong Kong, China*
[2]*Department of Electrical and Computer Engineering, University of Illinois, Urbana-Champaign, Illinois 61801, USA*
[*]*chchoy@eee.hku.hk*

**Abstract:** We investigate both optical and electrical properties of organic solar cells (OSCs) incorporating 2D periodic metallic back grating as an anode. Using a unified finite-difference approach, the multiphysics modeling framework for plasmonic OSCs is established to seamlessly connect the photon absorption with carrier transport and collection by solving the Maxwell's equations and semiconductor equations (Poisson, continuity, and drift-diffusion equations). Due to the excited surface plasmon resonance, the significantly nonuniform and extremely high exciton generation rate near the metallic grating are strongly confirmed by our theoretical model. Remarkably, the nonuniform exciton generation indeed does not induce more recombination loss or smaller open-circuit voltage compared to 1D multilayer standard OSC device. The increased open-circuit voltage and reduced recombination loss by the plasmonic OSC are attributed to direct hole collections at the metallic grating anode with a short transport path. The work provides an important multiphysics understanding for plasmonic organic photovoltaics.



**OCIS codes:** (310.6628) Subwavelength structures, nanostructures; (040.5350) Photovoltaic; (250.5403) Plasmonics; (310.6805) Theory and design.

## References and links

1. C. J. Brabec, S. Gowrisanker, J. J. M. Halls, D. Laird, S. J. Jia, and S. P. Williams, "Polymer-fullerene bulk-heterojunction solar cells," Adv. Mater. **22**, 3839–3856 (2010).
2. C. Deibel and V. Dyakonov, "Polymer-fullerene bulk heterojunction solar cells," Rep. Prog. Phys. **73**, 096401 (2010).
3. S. A. Maier, *Plasmonics: Fundamentals and Applications* (Springer, 2007).
4. X. H. Chen, C. C. Zhao, L. Rothberg, and M. K. Ng, "Plasmon enhancement of bulk heterojunction organic photovoltaic devices by electrode modification," Appl. Phys. Lett. **93**, 123302 (2008).
5. F. C. Chen, J. L. Wu, C. L. Lee, Y. Hong, C. H. Kuo, and M. H. Huang, "Plasmonic-enhanced polymer photovoltaic devices incorporating solution-processable metal nanoparticles," Appl. Phys. Lett. **95**, 013305 (2009).
6. J. L. Wu, F. C. Chen, Y. S. Hsiao, F. C. Chien, P. L. Chen, C. H. Kuo, M. H. Huang, and C. S. Hsu, "Surface plasmonic effects of metallic nanoparticles on the performance of polymer bulk heterojunction solar cells," ACS Nano **5**, 959–967 (2011).
7. J. Yang, J. B. You, C. C. Chen, W. C. Hsu, H. R. Tan, X. W. Zhang, Z. R. Hong, and Y. Yang, "Plasmonic polymer tandem solar cell," ACS Nano **5**, 6210–6217 (2011).
8. D. D. S. Fung, L. F. Qiao, W. C. H. Choy, C. D. Wang, W. E. I. Sha, F. X. Xie, and S. L. He, "Optical and electrical properties of efficiency enhanced polymer solar cells with Au nanoparticles in a PEDOT-PSS layer," J. Mater. Chem. **21**, 16349–16356 (2011).

#158715 - $15.00 USD Received 23 Nov 2011; revised 5 Jan 2012; accepted 5 Jan 2012; published 20 Jan 2012

9. F. X. Xie, W. C. H. Choy, C. C. D. Wang, W. E. I. Sha, and D. D. S. Fung, "Improving the efficiency of polymer solar cells by incorporating gold nanoparticles into all polymer layers," Appl. Phys. Lett. **99**, 153304 (2011).
10. C. C. D. Wang, W. C. H. Choy, C. Duan, D. D. S. Fung, W. E. I. Sha, F. X. Xie, F. Huang, and Y. Cao, "Optical and electrical effects of gold nanoparticles in the active layer of polymer solar cells," J. Mater. Chem. **22**, 1206–1211 (2011).
11. K. R. Catchpole and A. Polman, "Plasmonic solar cells," Opt. Express **16**, 21793–21800 (2008).
12. R. A. Pala, J. White, E. Barnard, J. Liu, and M. L. Brongersma, "Design of plasmonic thin-film solar cells with broadband absorption enhancements," Adv. Mater. **21**, 3504–3509 (2009).
13. H. A. Atwater and A. Polman, "Plasmonics for improved photovoltaic devices," Nat. Mater. **9**, 205–213 (2010).
14. W. E. I. Sha, W. C. H. Choy, and W. C. Chew, "Angular response of thin-film organic solar cells with periodic metal back nanostrips," Opt. Lett. **36**, 478–480 (2011).
15. W. E. I. Sha, W. C. H. Choy, Y. P. P. Chen, and W. C. Chew, "Optical design of organic solar cell with hybrid plasmonic system," Opt. Express **19**, 15908–15918 (2011).
16. W. E. I. Sha, W. C. H. Choy, Y. G. Liu, and W. C. Chew, "Near-field multiple scattering effects of plasmonic nanospheres embedded into thin-film organic solar cells," Appl. Phys. Lett. **99**, 113304 (2011).
17. T. A. Davis and I. S. Duff, "An unsymmetric-pattern multifrontal method for sparse LU factorization," SIAM J. Matrix Anal. Appl. **18**, 140–158 (1997).
18. W. E. I. Sha, W. C. H. Choy, and W. C. Chew, "A comprehensive study for the plasmonic thin-film solar cell with periodic structure," Opt. Express **18**, 5993–6007 (2010).
19. S. Selberherr, *Analysis and Simulation of Semiconductor Devices* (Springer, 1984).
20. L. J. A. Koster, E. C. P. Smits, V. D. Mihailetchi, and P. W. M. Blom, "Device model for the operation of polymer/fullerene bulk heterojunction solar cells," Phys. Rev. B **72**, 085205 (2005).
21. D. W. Sievers, V. Shrotriya, and Y. Yang, "Modeling optical effects and thickness dependent current in polymer bulk-heterojunction solar cells," J. Appl. Phys. **100**, 114509 (2006).
22. J. Y. Wang, F. J. Tsai, J. J. Huang, C. Y. Chen, N. Li, Y. W. Kiang, and C. C. Yang, "Enhancing InGaN-based solar cell efficiency through localized surface plasmon interaction by embedding Ag nanoparticles in the absorbing layer," Opt. Express **18**, 2682–2694 (2010).
23. X. F. Li, N. P. Hylton, V. Giannini, K. H. Lee, N. J. Ekins-Daukes, and S. A. Maier, "Bridging electromagnetic and carrier transport calculations for three-dimensional modelling of plasmonic solar cells," Opt. Express **19**, A888–A896 (2011).
24. P. Langevin, "Recombinaison et mobilites des ions dans les gaz," Ann. Chim. Phys **28**, 433–530 (1903).
25. L. Onsager, "Initial recombination of ions," Phys. Rev. **54**, 554–557 (1938).
26. C. L. Braun, "Electric-field assisted dissociation of charge-transfer states as a mechanism of photocarrier production," J. Chem. Phys. **80**, 4157–4161 (1984).
27. P. Boland, K. Lee, J. Dean, and G. Namkoong, "Design of organic tandem solar cells using low- and high-bandgap polymer:fullerene composites," Sol. Energy Mater. Sol. Cells **94**, 2170–2175 (2010).
28. Y. M. Nam, J. Huh, and W. H. Jo, "A computational study on optimal design for organic tandem solar cells," Sol. Energy Mater. Sol. Cells **95**, 1095–1101 (2011).

## 1. Introduction

As one of the promising candidates for photovoltaic applications, organic solar cells (OSCs) have drawn considerable attentions recently due to their properties in terms of light coupling and photocurrent generation, as well as the prospect of large-area production and low-cost processing [1, 2]. Many organic semiconductors exhibit very high absorption coefficient, making them promising for photovoltaic devices. However, the short lifetime and diffusion length of excitons result in ultrathin active-layer (typically few hundreds nanometers) configuration in OSCs. The configuration limits the light absorption efficiency, and thereby the power conversion efficiency. Having unique features of tunable resonance and unprecedented near-field concentration, plasmonics is an enabling technique for light manipulation and management [3].

Although various optical designs and physical mechanisms have been studied both experimentally [4–10] and theoretically [11–16] to improve the optical absorption of OSCs by incorporating metallic nanostructures, the effects of plasmonic nanostructures on the electrical properties of OSCs is still not fully understood. Hence, it is highly desirable to study the changes of electrical properties induced by plasmonic structures and the corresponding physics for OSCs, which will open a new way to design high-performance photovoltaics and explore novel functionalities of plasmonic nanodevices.

#158715 - $15.00 USD Received 23 Nov 2011; revised 5 Jan 2012; accepted 5 Jan 2012; published 20 Jan 2012

In this work, we develop a multiphysics model for plasmonic OSCs by solving the Maxwell's equations and semiconductor equations (Poisson, continuity, and drift-diffusion equations) with unified finite-difference method. Both the optical and electrical properties of OSCs incorporating a 2D metallic grating anode are investigated and analyzed. For typical active polymer materials, low hole mobility, which is about one magnitude smaller than electron mobility, dominates the electrical property of OSCs. Since surface plasmon resonances excited by the metallic grating will produce concentrated near-field penetrated into the active polymer layer and decayed exponentially away from the metal-polymer interface, a significantly nonuniform and extremely high exciton generation rate will be expected near the grating, which is also verified by our multiphysics model. Interestingly, we find that the reduced recombination loss and the increased open-circuit voltage can be achieved in plasmonic OSCs. The physical origin of the phenomena lies at direct hole collections to the metallic grating anode with a short transport path. In comparison with the plasmonic OSC, the hole transport in a 1D multilayer standard OSC experiences a long transport path and time because the standard planar OSC has a high exciton generation rate at the transparent front cathode. The unveiled multiphysics is particularly helpful for designing high-performance plasmonic organic photovoltaics.

## 2. Theoretical model

The multiphysics of plasmonic OSCs are governed by Maxwell's equations and semiconductor equations (Poisson, continuity, and drift-diffusion equations). The unified finite-difference (FD) approach is adopted to model both the optical and electrical properties of OSCs. Regarding both Maxwell's equations and semiconductor equations, the FD method will generate sparse matrices, which can be rapidly and efficiently inverted by the multifrontal algorithm [17].

For investigating optical properties of OSCs, the finite-difference frequency-domain method (FDFD) presented in our previous work [18] is employed to solve wave equations with the Yee lattice. The perfectly matched layer absorbing boundary condition is used to simulate the infinite air region implemented at the top and bottom sides of OSCs. With the aid of Floquet theorem, the periodic boundary condition is imposed at the left and right sides of OSCs for describing device structures with periodic metallic gratings. After obtaining electric-fields, the exciton generation rate can be written as

$$G(\mathbf{r}) = \int_{400\,\mathrm{nm}}^{800\,\mathrm{nm}} \frac{2\pi}{h} n_r(\lambda) k_i(\lambda) \varepsilon_0 |\mathbf{E}(\mathbf{r},\lambda)|^2 \Gamma(\lambda) d\lambda \tag{1}$$

where $h$ is the Planck constant, $n_c = n_r + ik_i$ is the complex refractive index of the active polymer material, $\mathbf{E}$ is the electric field, and $\Gamma$ is the solar irradiance spectrum of AM 1.5G. In view of a two-dimensional OSC structure, the Maxwell's equations can be decoupled into a TE and TM modes. Hence, the exciton generation rate is the average value of those for TE and TM polarizations.

For studying electrical properties of OSCs, one should self-consistently solve the coupled nonlinear semiconductor equations (Poisson, continuity, and drift-diffusion equations) given by [19–23]

$$\nabla \cdot (\varepsilon \nabla \phi) = -q(p - n) \tag{2}$$

$$\frac{\partial n}{\partial t} = \frac{1}{q} \nabla \cdot (-q\mu_n n \nabla \phi + qD_n \nabla n) + QG - (1 - Q)R \tag{3}$$

$$\frac{\partial p}{\partial t} = \frac{-1}{q} \nabla \cdot (-q\mu_p p \nabla \phi - qD_p \nabla p) + QG - (1 - Q)R \tag{4}$$

In the above, $\varepsilon$ is the dielectric constant of the polymer active material, $q$ is the electron charge, $\phi$ is the electrical potential, and $n$ ($p$) is the electron (hole) concentration. Moreover, $\mu_n$

#158715 - $15.00 USD Received 23 Nov 2011; revised 5 Jan 2012; accepted 5 Jan 2012; published 20 Jan 2012

($\mu_p$) is the electron (hole) mobility which can be described by field-dependent Frenkel-Poole form [2, 21], and $D_n$ ($D_p$) is the electron (hole) diffusion coefficient accessible by Einstein relations and mobilities. Furthermore, $\mathbf{J}_n = -q\mu_n n\nabla\phi + qD_n\nabla n$ and $\mathbf{J}_p = -q\mu_p p\nabla\phi - qD_p\nabla p$ are respectively electron and hole current densities, and $G$ is the exciton generation rate of Eq. (1) obtained with Maxwell's equations. Here, the recombination rate $R$ is taken as Langevin bimolecular form [24]; and the field-dependent exciton dissociation probability $Q$ is evaluated by Onsager-Braun theory [25, 26]. Using the Scharfetter-Gummel scheme in the spatial domain and using the semi-implicit strategy in the temporal domain [19], the 2D discretized forms of Eqs. (2), (3), and (4) are respectively given by

$$\begin{aligned}
&\frac{1}{\Delta_x^2}\varepsilon_{i+1/2,j}\phi_{i+1,j}^{t+1} + \frac{1}{\Delta_x^2}\varepsilon_{i-1/2,j}\phi_{i-1,j}^{t+1} + \frac{1}{\Delta_y^2}\varepsilon_{i,j+1/2}\phi_{i,j+1}^{t+1} + \frac{1}{\Delta_y^2}\varepsilon_{i,j-1/2}\phi_{i,j-1}^{t+1} \\
&- \left(\varepsilon_{i+1/2,j} + \varepsilon_{i-1/2,j} + \varepsilon_{i,j+1/2} + \varepsilon_{i,j-1/2}\right)\left(\frac{1}{2\Delta_x^2} + \frac{1}{2\Delta_y^2}\right)\phi_{i,j}^{t+1} - \frac{n_{i,j}^t + p_{i,j}^t}{U_t}\phi_{i,j}^{t+1} \\
&= q(n_{i,j}^t - p_{i,j}^t) - \frac{n_{i,j}^t + p_{i,j}^t}{U_t}\phi_{i,j}^t
\end{aligned} \tag{5}$$

$$\begin{aligned}
&\frac{n_{i,j}^{t+1} - n_{i,j}^t}{\Delta_t} = Q_{i,j}^t G_{i,j} - (1 - Q_{i,j}^t)R_{i,j}^t + \frac{D_{i+1/2,j}^n}{\Delta_x^2}B\left(\frac{\phi_{i+1,j}^{t+1} - \phi_{i,j}^{t+1}}{U_t}\right)n_{i+1,j}^{t+1} \\
&+ \frac{D_{i-1/2,j}^n}{\Delta_x^2}B\left(\frac{\phi_{i-1,j}^{t+1} - \phi_{i,j}^{t+1}}{U_t}\right)n_{i-1,j}^{t+1} + \frac{D_{i,j+1/2}^n}{\Delta_y^2}B\left(\frac{\phi_{i,j+1}^{t+1} - \phi_{i,j}^{t+1}}{U_t}\right)n_{i,j+1}^{t+1} \\
&+ \frac{D_{i,j-1/2}^n}{\Delta_y^2}B\left(\frac{\phi_{i,j-1}^{t+1} - \phi_{i,j}^{t+1}}{U_t}\right)n_{i,j-1}^{t+1} - \left[\frac{D_{i+1/2,j}^n}{\Delta_x^2}B\left(\frac{\phi_{i,j}^{t+1} - \phi_{i+1,j}^{t+1}}{U_t}\right)\right. \\
&+ \frac{D_{i-1/2,j}^n}{\Delta_x^2}B\left(\frac{\phi_{i,j}^{t+1} - \phi_{i-1,j}^{t+1}}{U_t}\right) + \frac{D_{i,j+1/2}^n}{\Delta_y^2}B\left(\frac{\phi_{i,j}^{t+1} - \phi_{i,j+1}^{t+1}}{U_t}\right) \\
&\left. + \frac{D_{i,j-1/2}^n}{\Delta_y^2}B\left(\frac{\phi_{i,j}^{t+1} - \phi_{i,j-1}^{t+1}}{U_t}\right)\right]n_{i,j}^{t+1}
\end{aligned} \tag{6}$$

$$\begin{aligned}
&\frac{p_{i,j}^{t+1} - p_{i,j}^t}{\Delta_t} = Q_{i,j}^t G_{i,j} - (1 - Q_{i,j}^t)R_{i,j}^t + \frac{D_{i+1/2,j}^p}{\Delta_x^2}B\left(\frac{\phi_{i,j}^{t+1} - \phi_{i+1,j}^{t+1}}{U_t}\right)p_{i+1,j}^{t+1} \\
&+ \frac{D_{i-1/2,j}^p}{\Delta_x^2}B\left(\frac{\phi_{i,j}^{t+1} - \phi_{i-1,j}^{t+1}}{U_t}\right)p_{i-1,j}^{t+1} + \frac{D_{i,j+1/2}^p}{\Delta_y^2}B\left(\frac{\phi_{i,j}^{t+1} - \phi_{i,j+1}^{t+1}}{U_t}\right)p_{i,j+1}^{t+1} \\
&+ \frac{D_{i,j-1/2}^p}{\Delta_y^2}B\left(\frac{\phi_{i,j}^{t+1} - \phi_{i,j-1}^{t+1}}{U_t}\right)p_{i,j-1}^{t+1} - \left[\frac{D_{i+1/2,j}^p}{\Delta_x^2}B\left(\frac{\phi_{i+1,j}^{t+1} - \phi_{i,j}^{t+1}}{U_t}\right)\right. \\
&+ \frac{D_{i-1/2,j}^p}{\Delta_x^2}B\left(\frac{\phi_{i-1,j}^{t+1} - \phi_{i,j}^{t+1}}{U_t}\right) + \frac{D_{i,j+1/2}^p}{\Delta_y^2}B\left(\frac{\phi_{i,j+1}^{t+1} - \phi_{i,j}^{t+1}}{U_t}\right) \\
&\left. + \frac{D_{i,j-1/2}^p}{\Delta_y^2}B\left(\frac{\phi_{i,j-1}^{t+1} - \phi_{i,j}^{t+1}}{U_t}\right)\right]p_{i,j}^{t+1}
\end{aligned} \tag{7}$$

where $B(x) = \frac{x}{e^x - 1}$ is the Bernoulli function and $U_t = \frac{k_B T}{q}$. It should be noted that the Gummel's method [19] has been incorporated in (5) to accelerate the convergence of the nonlinear

#158715 - $15.00 USD Received 23 Nov 2011; revised 5 Jan 2012; accepted 5 Jan 2012; published 20 Jan 2012

semiconductor equations. Since the dependent variables $(\phi, n, p)$ in the basic equations are of greatly different orders of magnitude and show a strongly different behaviors in regions with small and large space charge, the scaling procedure must be executed to guarantee the numerical stability of the algorithm [19]. Here, we redefine 5 independent basic units as listed in Table 1. Meanwhile, we keep the mathematical forms of nonlinear semiconductor equations unchanged.

Table 1. Scaled independent basic units. $\max\{\mathrm{DOS}\}$ denotes maximum effective density of states ($\mathrm{cm}^{-3}$).

| | |
|---|---|
| cm | $\max\{\mathrm{DOS}\}^{1/3}$ |
| s | $10^{12}$ |
| V | 1 |
| C | $\frac{1}{1.602\times10^{-19}}$ |
| K | $\frac{1}{300}$ |

The boundary conditions play a key role in modeling electrical properties of plasmonic OSCs. The potential boundary condition for the Shockley contact is given by

$$\phi = V_a - \frac{W_m}{q} \tag{8}$$

where $V_a$ is the applied voltage, and $W_m$ is the metal work function. For the ohmic contact, the built-in potential is the potential difference between the highest occupied molecular orbital (HOMO) of donor and lowest unoccupied molecular orbital (LUMO) of acceptor. The Neumann (floating) boundary condition is used to truncate the left and right boundaries of OSCs, i.e.

$$\frac{\partial \phi}{\partial N} = 0,\ \frac{\partial n}{\partial N} = 0,\ \frac{\partial p}{\partial N} = 0 \tag{9}$$

where $N$ are the normal vectors of the left and right boundaries of OSCs. The boundary conditions for the top and bottom electrodes can be written as

$$n = N_c \exp\left(-\frac{\psi_b^n}{k_B T}\right),\ \text{for cathode} \tag{10}$$

$$p = N_v \exp\left(-\frac{\psi_b^p}{k_B T}\right),\ \text{for anode} \tag{11}$$

where $N_c$ and $N_v$ are the effective density of states of electrons and holes, respectively. $\psi_b^n$ is the injection barrier between the LUMO and the cathode, and $\psi_b^p$ is the injection barrier between the HOMO and the anode.

The spatial steps of Maxwell's equations and semiconductor equations depend on the material wavelength and carrier Debye length, respectively. Regarding typical OSCs, we use the uniform grid to discretize Maxwell's equations and semiconductor equations with a spatial step of 1 nm. The time step of semiconductor equations can be evaluated by [19]

$$\Delta_t < \min\left(\frac{C\varepsilon}{\mu_n \cdot n + \mu_p \cdot p}\right) \tag{12}$$

where $C$ is a tunable constant. For OSCs, $C \approx 100$ from our numerical results.

#158715 - $15.00 USD Received 23 Nov 2011; revised 5 Jan 2012; accepted 5 Jan 2012; published 20 Jan 2012

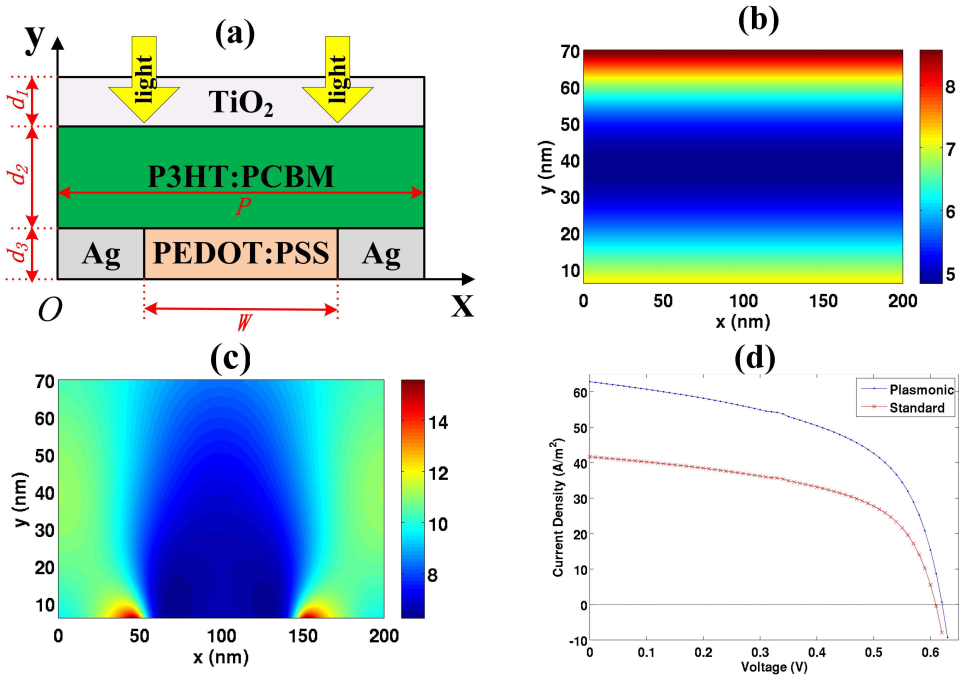


Fig. 1. (a) The schematic unit cell structure of a plasmonic OSC with 2D periodic metallic back grating as an anode. The geometric parameters are set as: $d_1 = 30$ nm, $d_2 = 70$ nm, $d_3 = 30$ nm, $W = 100$ nm, and $P = 200$ nm. The effective bandgap and density of states of the active material P3HT:PCBM is 1.1 eV and $2.5 \times 10^{19}\text{cm}^{-3}$. The anode of the Ag–PEDOT:PSS–Ag periodic grating is assumed to be an ohmic contact (no injection barrier). The $TiO_2$ cathode layer has an injection barrier of 0.2 eV. (b) The exciton generation rate ($\times 10^{27}$) of the standard OSC that replaces the Ag–PEDOT:PSS–Ag grating by a PEDOT:PSS layer. (c) The exciton generation rate ($\times 10^{27}$) of the plasmonic OSC. (d) The current density-voltage curves of the plasmonic and standard OSCs under the AM 1.5G light illumination.

## 3. Results and discussions

Figure 1(a) shows the schematic pattern of a bulk-heterojunction OSC. The P3HT:PCBM is used as a blend active layer. The cathode and anode of the OSC comprise the transparent and conductive material $TiO_2$ and the Ag–PEDOT:PSS–Ag (lateral) grating layer, respectively. The standard cell, which replaces the Ag–PEDOT:PSS–Ag grating layer by a PEDOT:PSS flat layer, is also modeled. The device parameters used in the simulation can be found in [27,28]. Figures 1(b) and (c) show the exciton generation rates in the active layer by solving Maxwell's equations. Critically from the standard cell that shows high exciton generation rate near the transparent cathode, the plasmonic cell exhibits very dense exciton generation near the Ag grating anode. Figure 1(d) shows the corresponding current density-voltage (J-V) curves. Table 2 lists the main characteristic parameters of plasmonic and standard cells. A significant improvement (50% increase) in the short-circuit current can be observed in the plasmonic OSC, which is attributed to the excited surface plasmon resonance for the TM wave and the light trapping effect for the TE wave induced by the metallic grating nanostructure. More intriguingly, the plasmonic grating structure does not reduce the open-circuit voltage of OSCs qualitatively but increases it a bit. The interesting phenomenon seems not to be intuitively understood because

#158715 - $15.00 USD Received 23 Nov 2011; revised 5 Jan 2012; accepted 5 Jan 2012; published 20 Jan 2012

more nonuniform and denser exciton generation occurs in the plasmonic cell leading to locally enlarged bimolecular recombination rate proportional to electron and hole concentrations at the initial time. However, the open-circuit voltage depends on the spatially averaged recombination loss at the steady case but not the initial recombination rates. The locally boosted recombination rates at the initial time still can yield smaller recombination loss if the transport path of photogenerated carriers are significantly shortened. In other words, fast collection time of carriers hopping from generation sites to electrodes could reduce recombination loss and thus induces larger open-circuit voltage. For a typical class of organic materials, such as P3HT:PCBM, hole mobility is about one magnitude smaller than electron mobility. Hence, the sweep-out or collection time to electrode is particularly unbalanced for electrons and holes. Having slow collection time, the hole transport will determine the recombination loss of OSCs. On one hand, the grating anode in the plasmonic cell strongly enhances the exciton generation rate nonuniformly distributed near the metal grating due to the exponentially decayed surface plasmon waves away from the Ag/P3HT:PCBM interface. On the other hand, the grating anode facilitates the hole collection with a very short transport path and hopping time. Contrarily, the hole transport in the standard cell experiences a long path because of the high exciton generation rate near the cathode.

Table 2. The characteristic parameters of plasmonic and standard OSCs involving short-circuit current $J_{sc}$, open-circuit voltage $V_{oc}$, maximum power (MP), fill factor (FF), and power conversion efficiency (PCE).

| Plasmonic | $J_{sc}$ ($A/m^2$) | $V_{oc}$ (V) | MP (W) | FF | PCE (%) |
|---|---|---|---|---|---|
| | 62.84 | 0.62 | 21.47 | 0.55 | 2.15 |
| Standard | $J_{sc}$ ($A/m^2$) | $V_{oc}$ (V) | MP (W) | FF | PCE (%) |
| | 41.67 | 0.61 | 14.03 | 0.55 | 1.40 |

Table 3. An overview of voltage, current density, exciton dissociation probability (Diss), and recombination loss (Rec loss) at short-circuit (SC), maximum power (MP), and open-circuit (OC) conditions.

| Plasmonic | V (V) | J ($A/m^2$) | $\langle$Diss$\rangle$ (%) | $\langle$Rec loss$\rangle$ (%) |
|---|---|---|---|---|
| SC | 0 | 62.84 | 66.96 | 2.62 |
| MP | 0.48 | 44.73 | 58.97 | 14.55 |
| OC | 0.62 | 0 | 55.47 | 80.88 |
| Standard | V (V) | J ($A/m^2$) | $\langle$Diss$\rangle$ (%) | $\langle$Rec loss$\rangle$ (%) |
| SC | 0 | 41.67 | 66.96 | 3.18 |
| MP | 0.47 | 30.42 | 59.19 | 14.93 |
| OC | 0.61 | 0 | 55.75 | 81.91 |

To demonstrate this point, we calculate the spatially averaged exciton dissociation probability and recombination loss at the steady state [20] as listed in Table 3. The averaged recombination loss can be defined as

$$\langle R_{loss} \rangle = 1 - \frac{\langle U \rangle}{\langle QG \rangle} \tag{13}$$

where $U = QG - (1-Q)R$ is the net generation rate. The recombination loss of the plasmonic cell is smaller than that of the standard cell with larger photovoltages at maximum power and open-circuit conditions. To further confirm our argument, we define dummy exciton generation

#158715 - $15.00 USD Received 23 Nov 2011; revised 5 Jan 2012; accepted 5 Jan 2012; published 20 Jan 2012

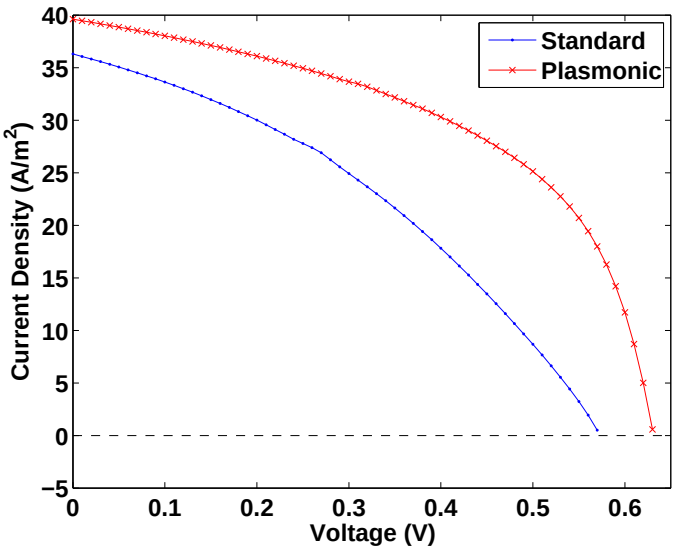


Fig. 2. The J-V curves of the plasmonic and standard OSCs with extremely nonuniform exciton generation rate and unbalanced electron/hole mobilities.

rates for the plasmonic and standard cells respectively as

$$G_{grating} = \begin{cases} G_c, & d_3 \le y \le d_3 + L_g \\ 0, & \text{else} \end{cases} \tag{14}$$

$$G_{planar} = \begin{cases} G_c, & d_3 + d_2 - L_g \le y \le d_3 + d_2 \\ 0, & \text{else} \end{cases} \tag{15}$$

where $G_c = 2.14 \times 10^{28} \mathrm{m}^{-3}\mathrm{s}^{-1}$ and $L_g = 20\,\mathrm{nm}$. Here, we remove the amplitude difference in exciton generation rates between plasmonic and standard OSCs and enlarge the nonuniform feature of the exciton generation. For the dummy case, the hole mobility is set to be two order of magnitude lower than electron mobility resulting in the increased recombination loss. We recalculate the J-V curves of the plasmonic and standard OSCs as shown in Fig. 2. The significant drops in the open-circuit voltage and fill factor can be clearly observed for the standard cell due to undesirable hole collections with longer sweep-out time or hopping path. Thus the exciton generation should be carefully manipulated to reduce the recombination loss, increase the open-circuit voltage, and improve the fill factor. This is helpful to design high-performance organic photovoltaics particularly for those with the active material of unbalanced electron/hole mobilities.

## 4. Conclusion

We investigate the optical and electrical properties of OSCs with a metallic back grating as the anode. Due to favorite hole collections with the short transport path and sweep-out time, the recombination loss of the plasmonic OSC can be smaller than that of the standard cell leading to larger open-circuit voltage. The work establishes a multiphysics framework to seamlessly integrate optical with electrical properties of plasmonic OSCs. The physics unveiled is also useful for designing high-performance organic photovoltaics.

#158715 - $15.00 USD Received 23 Nov 2011; revised 5 Jan 2012; accepted 5 Jan 2012; published 20 Jan 2012

**Acknowledgments**

The authors acknowledge the support of the grants (Nos. 712010, 711609, and 711511) from the Research Grant Council (RGC) of the Hong Kong and the grant (No. 10401466) from the University Grant Council (UGC) of the University of Hong Kong. This project is also supported in part by a Hong Kong UGC Special Equipment Grant (SEG HKU09) and by the UGC of Hong Kong (No. AoE/P-04/08).

#158715 - $15.00 USD Received 23 Nov 2011; revised 5 Jan 2012; accepted 5 Jan 2012; published 20 Jan 2012